Available online at www.sciencedirect.com
SCIENCE DIRECT
Polymer 47 (2006) 3197–3206
polymer
www.elsevier.com/locate/polymer

Phase morphology and toughening mechanism of polyamide 6/EPDM-*g*-MA blends obtained via dynamic packing injection molding

Cong Wang, Juan Xia Su, Jiang Li, Hong Yang, Qin Zhang, Rong Ni Du, Qiang Fu *

State Key Laboratory of Polymer Materials Engineering, Department of Polymer Science and Materials, Sichuan University, ChengDu 610065, People's Republic of China

Received 16 November 2005; received in revised form 28 February 2006; accepted 5 March 2006

Abstract

One of the most important findings in polymer-toughening is known as the critical matrix ligament thickness (τ_c) theory, which is directly related to both rubber concentration and average size of particles. All these studies assume that rubber particles are spherical and randomly distributed in the matrix. Rubber particles may be stretched and oriented along the shear flow direction in real processing. In this paper the effect of stretched and oriented rubber particles on the impact strength of PA6/EPDM-*g*-MA blends have been studied via dynamic packing injection molding (DPIM). The impact strength of specimens obtained by DPIM was found substantially increase at all the blends investigated, compared with the one obtained via conventional injection molding. Particularly, more than 30 kJ m^{-2} increase of the impact strength was observed for specimens with a higher rubber content (more than 15 wt%). SEM results showed a remarkably decrease of rubber particle size and more uniform dispersion of the dynamic molded specimens. This can be attributed to the shear induced reaction at the interface between polyamide 6 and EPDM-*g*-MA during the packing stage. The rubber particles were found stretched along the melt shear flow direction when it is content above 15 wt%. A master curve can be also constructed by plotting the impact strength versus the inter-particle distance, indicating that Wu's criterion still works for blends with stretched and oriented rubber particles when the crack propagation direction is perpendicular to the orientation direction of rubber particles. The observed higher impact strength in dynamic specimens could be due to, in part, the enhanced flexural stiffness, which will absorb more energy during impact process when the fracture of IZOD bars is incomplete, but more importantly due to the existence of the stretched and oriented rubber particles, which are more efficient in slowing the velocity of crack propagation and thus cause higher impact resistance when the fracture propagation direction is perpendicular to the rubber oriented direction.

Keywords: PA6/EPDM-*g*-MA blends; Shear; Stretched and oriented rubber particles

1. Introduction

Polyamides, as other semi-crystalline polymers, such as isotactic polypropylene and linear polyethylene, are notch sensitive because of their low resistance to crack propagation, which leads to embrittlement at high strain rate or low temperature. A lot of work has been done on the toughening of polyamides by incorporation of fine particles, particularly, by using rubber particles [1–12]. Most of these studies focused on two parameters, rubber particle size [3,8] and rubber concentration [8], until Wu combined these two interdependent parameters into one parameter, inter-particle distance or inter-particle ligament thickness (τ_c) [1]. A sharp brittle to ductile transition occurs when the inter-particle distance is below a critical value, which is just a specific material characteristic. The theory, which has also created much controversy, has been further clarified by Muratoglu et al. [9,10,13]. They proposed that specially oriented crystalline layers perpendicular to the interface would prevent premature fracture when these layers percolated over the whole material. And furthermore, Wu's theory has a prerequisite: the rubber particles are considered as spherical and randomly distributed in the matrix. If the rubber particles are stretched and oriented, the stress field around a particle will be more complicated than that of spherical rubber particles, does the τ_c criterion still work? So it is interesting to control not only the rubber particle size and rubber content but also the particle shape to fully understand the toughening mechanism. The shape of rubber in polymer matrix is influenced by the following four factors [16–27]: (1)

* Corresponding author. Tel.: +86 28 854 05402.
E-mail address: qiangfu@scu.edu.cn (Q. Fu).

0032-3861/$ - see front matter © 2006 Elsevier Ltd. All rights reserved.
doi:10.1016/j.polymer.2006.03.012

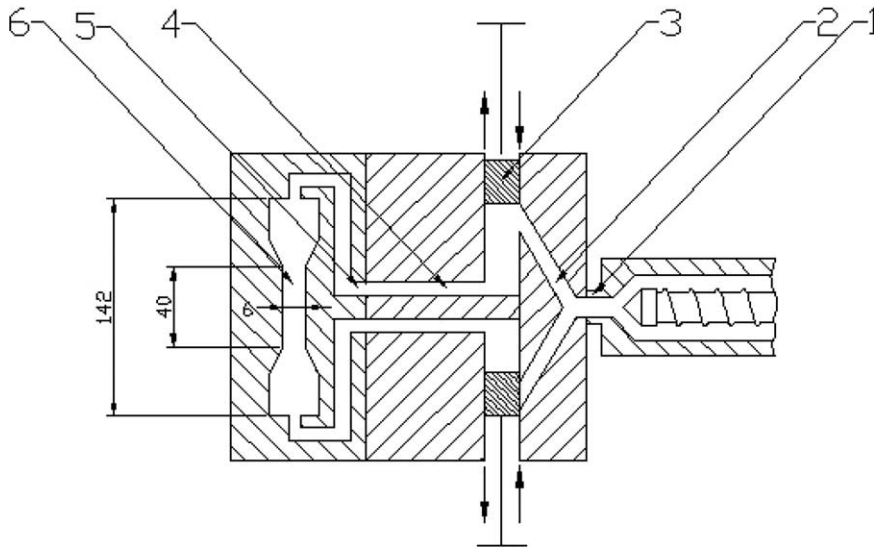

Fig. 1. The schematic representation of dynamic packing injection molding: (1) nozzle, (2) sprue, (3) piston, (4) runner, (5) connector, (6) specimen.

processing conditions; (2) blends composition; (3) interface interaction; (4) viscosity ratio of the components.

In recent years, dynamic packing injection molding (DPIM) had been found to be a very effective way of controlling polymer morphology [28–32]. The main feature of DPIM is after the melt was injected into the mold it is forced to move repeatedly in a chamber by two pistons moving reversibly with the same frequency, because of the shear field induced by pistons, a multi-layer specimen was obtained during the solidification progress. In this work, the effect of stretched and oriented rubber particles via DPIM on the impact strength of PA6/EPDM-*g*-MA blends was investigated. Our purpose is to verify whether Wu's criterion still works for blends with stretched and oriented rubber particles along the shear flow direction and to find out in what way will the stretched and oriented rubber particles affect the impact strength of PA6/EPDM-*g*-MA blends.

2. Experimental

2.1. Material and specimen preparation

Studies were performed on blends based on a commercial grade of polyamide 6(B3S, BASF) and ethylene–propylene–diene monomer grafted with maleic anhydride (CG700, ChenGuang chemical institution) with a grafted rate of 0.92%. The melt flow index (MFI at 230 °C and 2.16 kg load) and density of polyamide 6 were 36 g/10 min and 1.13 g/cm^3, respectively, while that of EPDM-*g*-MA were 5 g/10 min (230 °C and 2.16 kg load) and 0.84 g/cm^3, respectively. Blends were prepared in different proportion of polyamide 6 with 5, 10, 15, 20, 30, 40 wt% of the EPDM-*g*-MA in a TSSJ-2S co-rotating twin-screw extruder. The barrel temperature and the screw speed were set at 190–220–230–230–220 °C and 120 rpm, respectively. While the droplets got from extruder were molded both with DPIM and traditional injection molding for comparison under the same processing parameter. The schematic representation of DPIM is shown in Fig. 1. The obtained specimens are dumbbell shape. The shear rate is about 10 s^{-1} calculated from the geometry of mold. The specimens obtained from DPIM and traditional injection moldings are called dynamic specimens and static specimens, respectively. The processing parameters in DPIM are listed in Table 1. Prior to extrusion and injection molding the materials were vacuum oven-dried for 24 h at 80 °C.

2.2. Mechanical testing

The central part of specimens (40×6×3.5 mm^3) which was not standard was used for impact testing. The notches with 45° were made at a depth of 1 mm thus the depth of the remaining part was 5.0 mm. The impact experiment was carried out on an I200XJU-2.75 Impact Tester according to ISO 180. The fracture propagation direction is perpendicular to the melt shear flow direction. Since the blends with rubber content higher than 15 wt% are of very high toughness, the fracture is incomplete. The IZOD bars bend and the pendulum swings by. In this case, only the area of the fractured part was used for calculation and the un-fractured part was deducted. Flexural properties were determined in three-point bending mode in an RG T-10 University Testing Machine according to ASTM

Table 1
Processing parameter in DPIM

Processing parameter	Parameter value
Injection pressure (MPa)	90
Packing pressure (MPa)	50
Melt temperature (°C)	240
Mold temperature (°C)	20
Dynamic packing pressure (MPa)	35
Dynamic packing frequency (Hz)	0.3

standard D790. The crosshead speed and span distance used were 2 mm min^{-1} and 70 mm, respectively. The values of all the mechanical parameters were calculated as averages over 6–9 specimens for each composition.

2.3. Wide-angle X-ray diffraction (WAXD)

The WAXD experiments were conducted with a siemens D500 diffractometer. The wavelength of the monochromated X-ray from Cu K_α radiation is 0.154 nm and the reflection mode was used. The scanning 2θ range was 5–40° with a scanning rate of 5°/min.

2.4. Differential scanning calorimetry (DSC)

The melting behavior of both dynamic and static specimens was studied on a Perkin–Elmer DSC Priys-1. The instrument was calibrated using indium as standard. Melting endotherms were recorded at 10 °C min^{-1} heating rate from 4 to 5 mg specimen in a nitrogen atmosphere. The degree of crystallinity was calculated from heat of fusion using 190 J g^{-1} as the heat of fusion of 100% crystalline polyamide 6 [33].

2.5. Scanning electron microscope (SEM)

The specimens were cryogenically fractured perpendicular to the shear flow direction and parallel to the shear flow direction in liquid nitrogen, called T and F direction, respectively. Then the cryogenically fractured specimens were etched in boiled toluene for 1 h to selectively dissolve the rubber particles. After the surface was coated with gold powder the phase morphology was observed in a Hitachi X-650 SEM instrument operating at an accelerating voltage of 5 kV.

3. Results

3.1. Mechanical properties

Fig. 2 shows the impact strength of dynamic and static specimens as a function of rubber content. For pure polyamide 6, the result that the impact strength is nearly the same for dynamic and static specimens implies the orientation of polyamide 6 macromolecules along shear flow direction is difficult due to very low melt viscosity and the strong interaction between macromolecules caused by hydrogen-bonds [34]. This is different from that for pure polypropylene [35] and polyethylene [32] for which the orientation of macromolecules was obvious and remarkable increase of impact strength was seen for these specimens when the fracture propagation direction was perpendicular to the orientation direction. So in this case, any obvious change of the impact strength in PA6/EPDM-*g*-MA blends should mainly attribute to the contribution of the rubber. As shown in Fig. 2, for the specimens obtained by conventional injection molding, a sharp brittle–ductile transition occurs at 10–20 wt% of rubber content. The toughness becomes independent of rubber content when rubber content is more than 20 wt%. This can be well

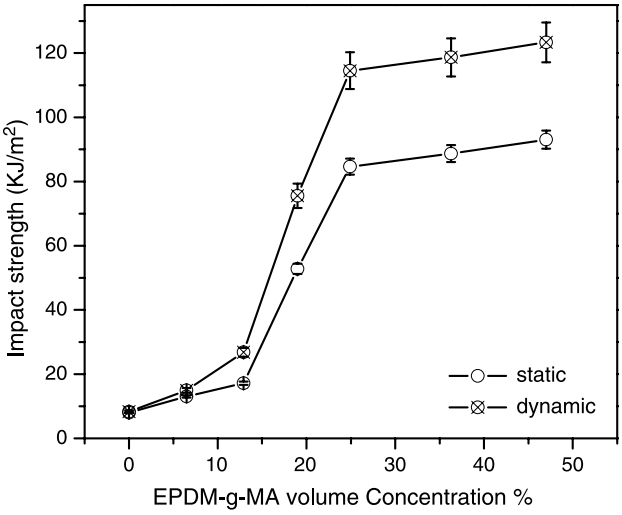

Fig. 2. The curve of the impact strength versus the content of EPDM-*g*-MA.

understood by using Wu's critical matrix-ligament thickness theory. The impact strength of specimens obtained by DPIM is about 30 kJ m^{-2} higher than that of specimens via conventional injection molding at a higher rubber content (more than 15 wt%). Unlike the phenomenon of brittle–ductile–brittle transition observed for dynamic specimens of PP/EPDM blends via DPIM [31], only brittle to ductile transition is seen for both dynamic and static specimens of PA6/EPDM-*g*-MA blends.

Since the flexural property could also affect the impact strength, particularly when the fracture of IZOD bars is incomplete, the flexural strength and modulus of the samples were measured and the result is listed in Table 2. For PA6 and its blends, the flexural modulus of dynamic specimens is about 0.1 GPa higher than that of static ones. A similar trend to that of the flexural modulus is again observed for the flexural strength, albeit not significantly.

3.2. Phase morphology

The static specimens can be usually divided into two parts called skin layer and core layer. In contrast to the static specimens, the dynamic ones were departed into three parts with a shear layer existing between skin layer and core layer. However, since the skin layer takes only very small part of the

Table 2
Flexural properties PA6 and its blends by different injection moldings

Flexural properties	Composition		
	PA6	PA6/EPDM-*g*-MA (80/20)	PA6/EPDM-*g*-MA (60/40)
E-modulus (GPa)			
Dynamic	1.309	1.056	0.746
Static	1.185	0.953	0.632
Strength (MPa)			
Dynamic	40.60	31.62	20.57
Static	37.30	28.84	18.16

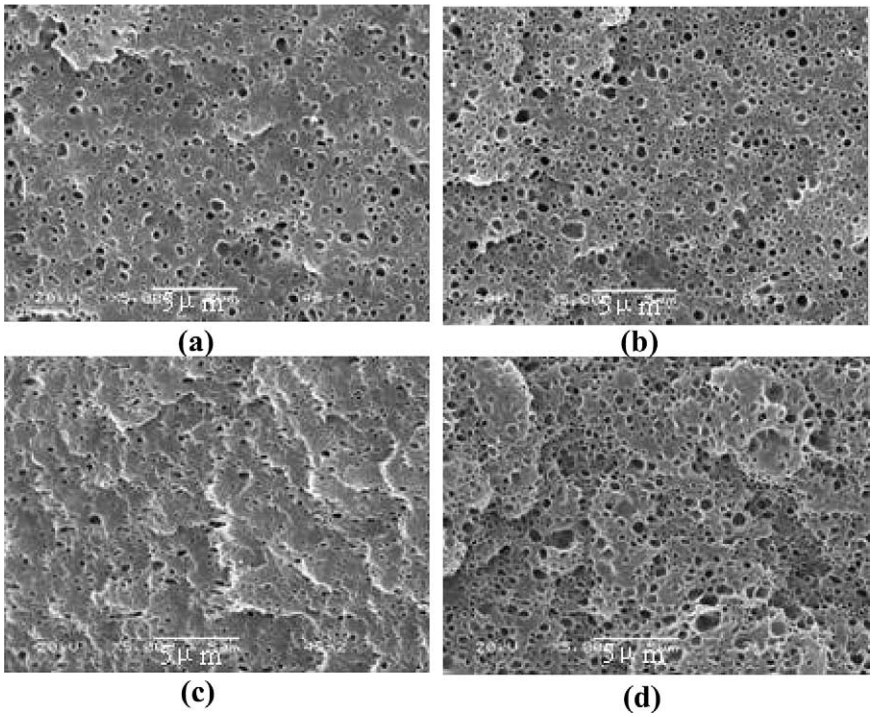

Fig. 3. The SEM photographs got from the core layer of static specimens; (a) and (b) are from T direction, (c) and (d) are from F direction; (a) and (c) got from blends with 20 wt% rubber content, (b) and (d) got from blends with 40 wt% rubber content.

specimens and also due to the similarity of phase morphology and crystal structure in this layer between the dynamic and static specimens, we mainly focus our attention on the shear layer and the core and ignore the skin layer in all our discussion.

The phase morphology of static specimens in the core layer at T direction and F direction are shown in Fig. 3. The black domains represent the position of the extracted rubber phase. From these micrographs it is obvious that only sea-island structure exists in the composition investigated. The rubber size is seen not much changed as increasing of rubber content. It is about 0.4–0.5 μm. Combining the phase morphology at these two directions one can conclude that for static specimens the dispersed rubber particles are spherical in the composition investigated.

For the phase morphology of dynamic specimens, the shear layer and the core layer were also examined at both T and F direction. The phase morphologies at T direction are shown in Fig. 4. One observes in this direction always spherical dispersed rubber particles. Again, the rubber size is seen not much changed as increasing of rubber content. But compared with static specimens, the rubber size shows remarkable decrease and drops down to 0.35 in the core and 0.25 μm in the shear layer, respectively. This can be attributed to the shear induced reaction at the interface between polyamide 6 and EPDM-*g*-MA during packing process, which provides additional chance for polyamide 6 and EPDM-*g*-MA to interact at interface. The larger size in the core compared with that in the shear layer may be due to the longer relaxation time in the core, where the specimens are frozen at last.

The stretched particles in the shear layer are seen for dynamic specimens at F direction when the rubber content is more than 15 wt%, as shown in Fig. 5. Due to lower viscosity of the blends while the rubber content below 15 wt%, the dispersed rubber particles keep spherical although the domain size of the dispersed rubber particles is larger than that of blends with rubber content above 15 wt%. When rubber content excesses 15 wt%, besides the sphere, some cigar-like dispersed particles oriented along the shear flow direction are also observed. According to the equation $\tau = \eta^*\gamma$, shear stress τ is proportional to the viscosity. Since the viscosity of the blends increases as increasing of rubber content, a higher shear force is expected for specimens with higher rubber content. So one observes stretched rubber particles at high rubber content. Seen from Fig. 5 one can also find that even at high rubber content the rubber particles remain spherical in the core layer at F direction. This may be attributed either to the elastic recovery and/or the breaking up of the cigar-like particles of the rubbery phase according to the Rayleigh–Taylor–Tomotika theory [22]. The average rubber particle size and particle size polydispersity obtained by image analysis are listed in Table 3.

3.3. Crystal structure

Since polyamide 6 can exist in several polymorphous crystalline phases, one has to ask whether the mentioned increase of impact strength is related to a change of crystal

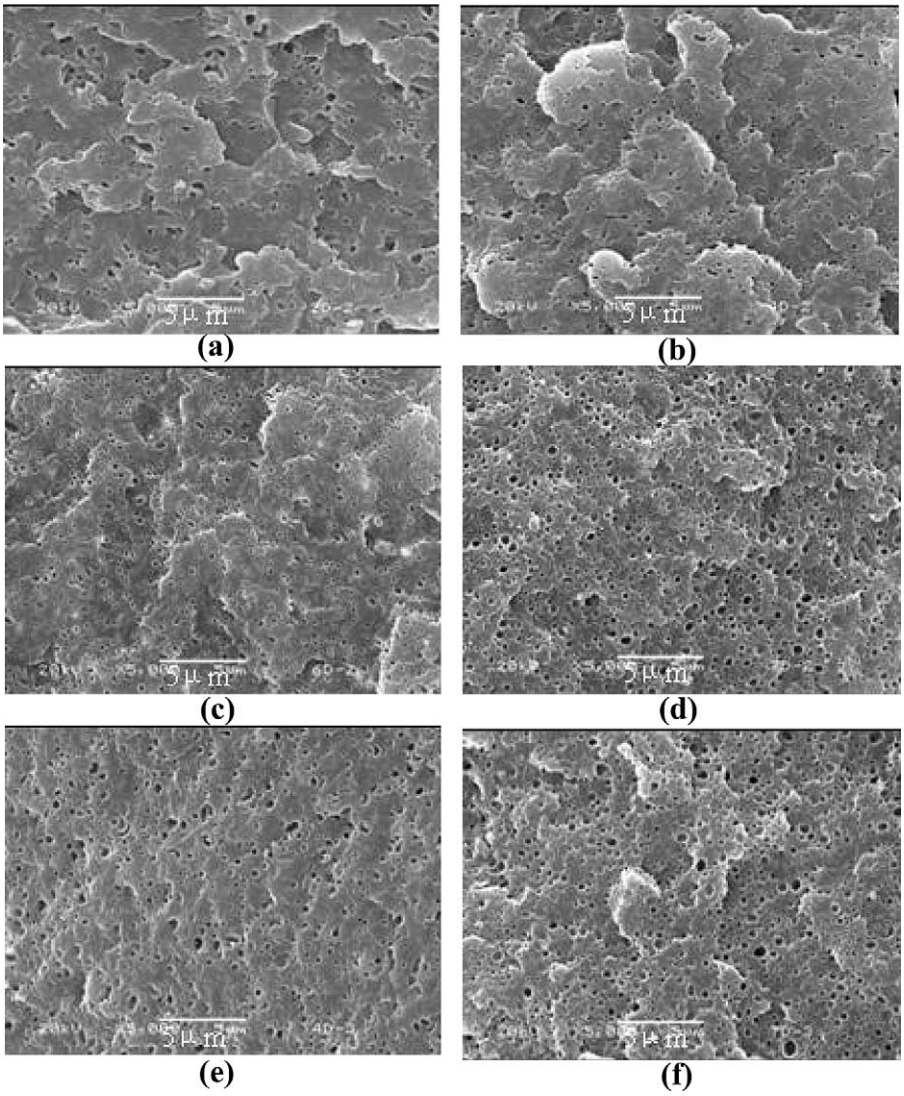

Fig. 4. The SEM photographs of PA6/EPDM-*g*-MA blends at T direction; (a)–(d) are from the shear layer of dynamic specimens with 10, 20, 30 and 40 wt% rubber content, respectively; (e) and (f) are from the core layer of dynamic specimens with 20 and 40 wt% rubber content, respectively.

structure induced via shear stress. For this reason, we carried out WAXS experiments for all the composition studied. The WAXD results of selected specimens are shown in Fig. 6. Peaks at 20.5 and 23.5° can be assigned to (200) and the (002) planes of the α phase, respectively. The peak around 21.5° is characteristic of the γ phase belong to (200) and (101) planes. Comparing dynamic specimens to static ones, no matter whether the rubber exists or not, one can find that dynamic specimens have more content of γ phase and less content of α phase. However, α phase gives higher impact strength than γ phase [36]. Hence, the improvement of the impact strength of dynamic specimens is not caused by the change of crystalline structure.

3.4. Crystallinity and melting point

Since the crystallinity of polyamide 6 will also contribute, at certain degree, to the observed change of impact strength. So we carried out DSC experiment to measure crystallinity of the blends as function of rubber content for both dynamic and static specimens. The melting curves of shear and core layers of dynamic specimens and that of core layer of static ones were shown in Fig. 7. One expects two melting temperatures, which were for α phase and γ phase, respectively. However, only one melting peak around 220 °C was seen for each layer of these specimens, which corresponding to the melting of α phase. Two possibilities exist: one is that γ phase had been transferred into α phase during heating; the other is that the content of γ phase is very small and it is melting cannot be detected by DSC. The crystallinity is calculated from the equation:

$$\text{Crystallinity} = \frac{\Delta H_f}{\Delta H_f^m \chi_A} \times 100\% \quad (1)$$

where ΔH_f is the enthalpy of polyamide 6 for the blends, ΔH_f^m is the enthalpy of polyamide 6 whose crystallinity is

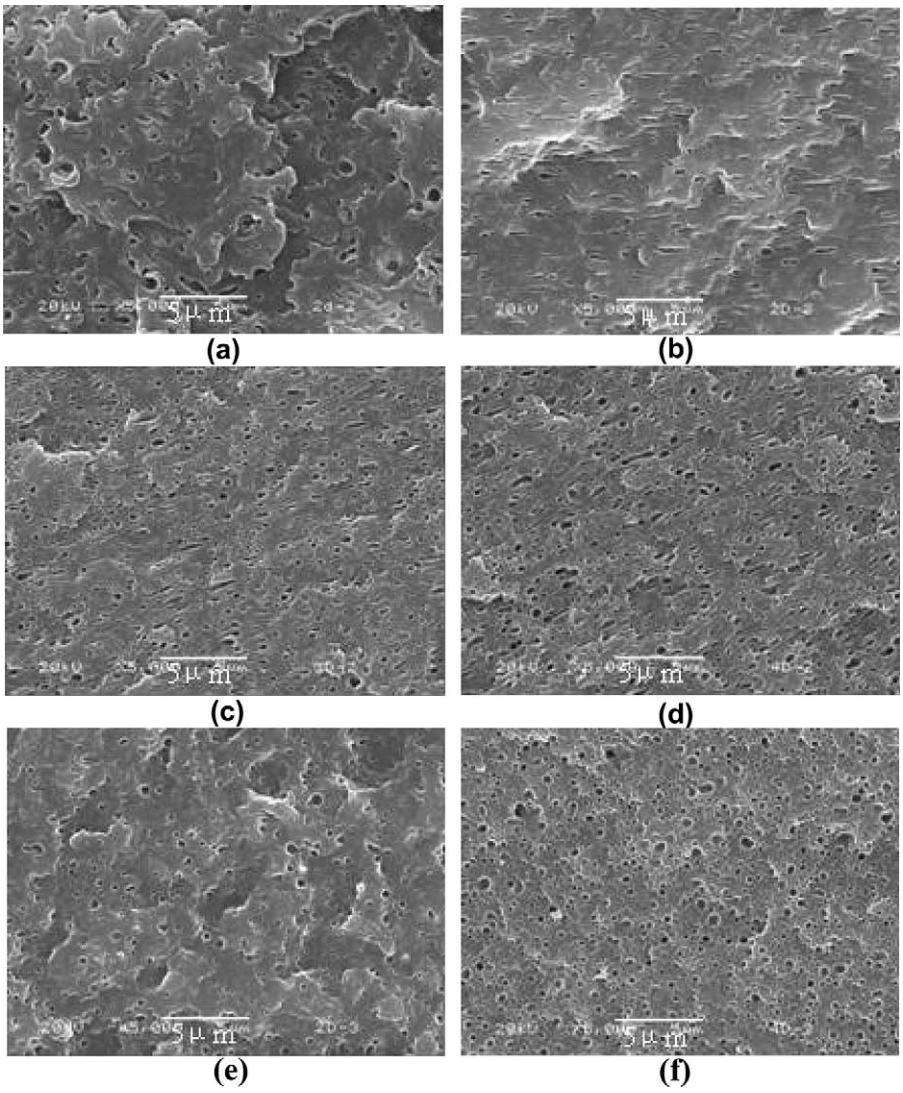

Fig. 5. The SEM photographs got from dynamic specimens at F direction; (a)–(d) are from the shear layer of blends with 10, 20, 30 and 40 wt% rubber content, respectively; (e) and (f) are from the core layer of blends with 20 and 40 wt% rubber content, respectively.

100%, the literature value 190 J g^{-1} is used (α phase). χ_A is the content of polyamide 6 for the blends. Fig. 8 shows the melting point and crystallinity of the dynamic specimens in different layers and the static specimens in core layer. One observes constant crystallinity and melting point within the whole composition region investigated, which indicating that shear has no effect on these two parameters. So the observed change of impact strength has nothing to do with the change of crystallinity and melting point of polyamide/EPDM-*g*-MA blends produced by DPIM.

4. Discussion

Seen from results above, the crystallinity, melting point and the change of crystalline structures do not contribute to the improvement of impact strength of dynamic specimens. Also, the orientation of polyamide 6 macromolecules does not contribute to the impact strength of the blends. Thus, the difference of the impact strength between dynamic and static specimens should be only attributed to the difference of phase morphology.

Table 3
The average particle sizes and particle size polydispersity of PA6/EPDM-*g*-MA blends in transverse direction

Rubber weight content (%)	5	10	15	20	30	40
Rubber volume content (%)	6.5	12.9	19	24.9	36.3	47
Particle size (μm)						
D-shear	0.30	0.28	0.21	0.22	0.22	0.27
D-core	0.39	0.36	0.28	0.26	0.27	0.34
S-core	0.53	0.41	0.36	0.38	0.42	0.47
Polydispersity σ						
D-shear	1.36	1.34	1.28	1.26	1.24	1.24
D-core	1.39	1.36	1.32	1.32	1.28	1.29
S-core	1.46	1.40	1.36	1.34	1.39	1.45

D, dynamic specimens; S, static specimens.

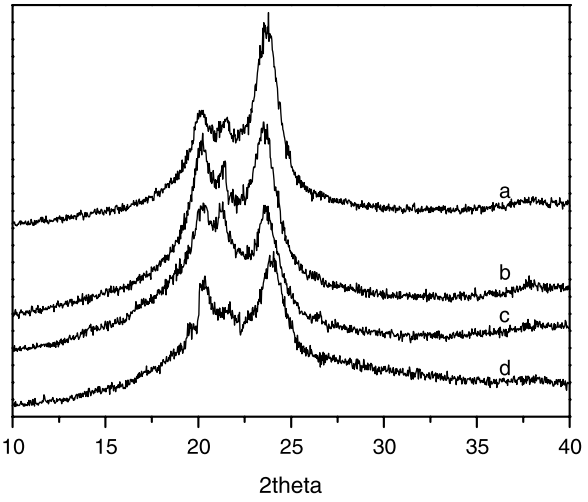

Fig. 6. WAXD photographs of blends; (a) and (d) are from core layer of static specimens without and with 40 wt% rubber content, respectively; (b) and (c) are from shear layer of dynamic specimens without and with 40 wt% rubber content, respectively.

4.1. The inter-particle distance

For polyamide 66/rubber blends studied by Wu, a simple cubic packing was chosen to approximate the real spatial arrangement of the rubber particles in polyamide matrix, the value τ of the inter-particle distance can be calculated from the equation [1]:

$$\tau = d\left[\left(\frac{\pi}{6V_f}\right)^{1/3} - 1\right] \tag{2}$$

with the assumption that the dispersed particles are spherical and of equal diameter, d. where V_f is volume fraction of these

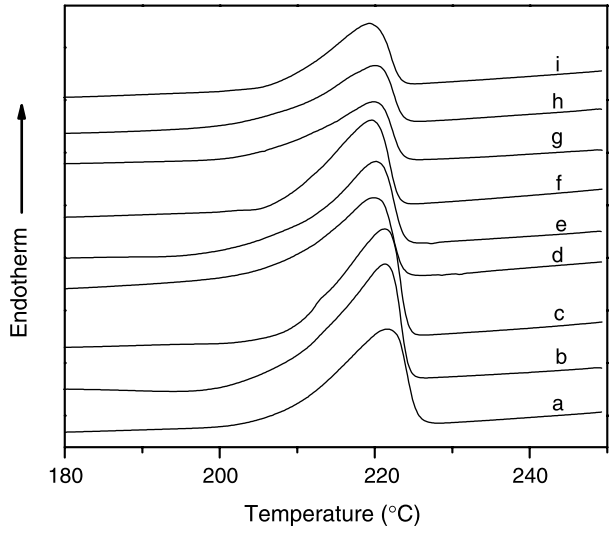

Fig. 7. DSC melting curve of pure PA6 and its blends: (a), (d) and (g) are from the shear layer while (b), (e) and (h) are from the core layer of dynamic specimens without and with 20 and 40 wt% rubber content, respectively; (c), (f) and (i) are from the core layer of static specimens without and with 20 and 40 wt% rubber content, respectively.

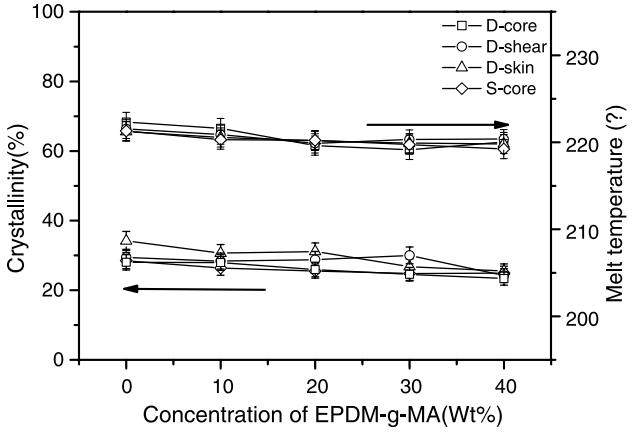

Fig. 8. The crystallinity and the melting point in different layers of PA6/EPDM-*g*-MA blends. D, dynamic specimen; S, static specimen.

particles. However, in real blends the particle sizes frequently obey a log–normal distribution [37]. The mean inter-particle distance for the blend that is polydisperse system can be described by [38]:

$$\tau = d\left[\left(\frac{\pi}{6V_f}\right)^{1/3} \exp\left(1.5\, ln^2\sigma\right) - \exp(0.5\, \ln^2\sigma)\right] \tag{3}$$

where σ is particle size distribution. Eq. (3) can be used for static specimens since the rubber particles are roughly spherical in the composition investigated. While for dynamic specimens, the cigar-like rubber particles oriented along the shear flow direction exist in the shear layer, particularly, for specimens with higher rubber content. Can Eq. (3) still be used to calculate the inter-particle distance τ? For dynamic specimens all the particles are circular observed at T direction. The values of particle size at this direction are used together with the values of particle size polydispersity to calculate the inter-particle distance. Noting that the particle size in shear layer is smaller than that in core layer, the average particle size of dynamic specimens is represented by number average values considering the area of the cross section of shear layer is two times larger than that of the core layer. Using the parameter listed in Table 3, the inter-particle distance can be worked out through Eq. (3). The plot of impact strength versus inter-particle distance is shown in Fig. 9. A sharp increase of impact strength happens when the inter-particle distance is lower than 0.28 μm for both dynamic and static specimens, indicating that Wu's theory still works by using the particle size got from T direction, as the fracture propagation direction is perpendicular to the rubber oriented direction. The master curve splits into two in the tough region. For polyamide/rubber blends Wu also found that in the range of $\tau < \tau_c$, the master curve split into separate branches where the level of impact energy depends on the actual composition of blend [1]. However, the split branches studied here cannot be attributed to composition of blends because the impact strength of dynamic specimens is higher than that of static ones under the same rubber content. It can be due to the contribution of the stretched and oriented rubber particles.

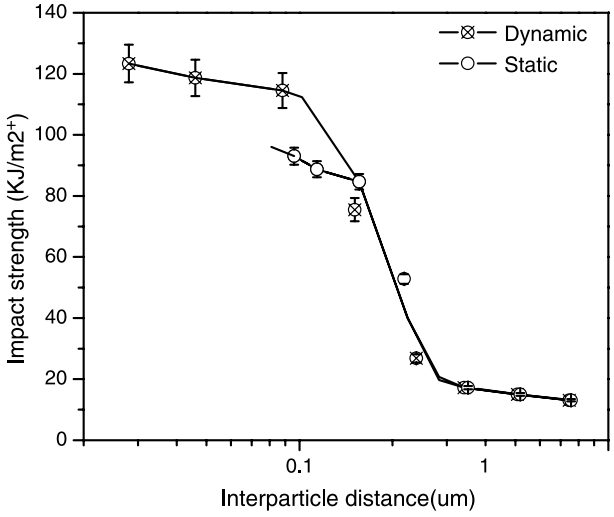

Fig. 9. The impact strength as a function of inter-particle distance of PA6/EPDM-*g*-MA blends.

4.2. The effect of stretched and oriented rubber particles on impact strength

There are two effects of DPIM on phase morphology of PA6/EPDM-*g*-MA blends, compared to that of conventional one: (1) smaller rubber particle size, (2) the existence of stretched and oriented rubber particles. Many studies have documented that blends with smaller particle size owe higher toughness under the same rubber content. What is the effect of stretched and oriented rubber particles on impact strength? On the one hand, the existence of stretched and oriented rubber particles in dynamic specimens indicates that the flexural stiffness should be higher in these specimens than that of static ones. This is agreed with the experimental results of flexural testing. When IZOD bars are of high toughness, the fracture is incomplete and they bend to let the pendulum swings by during impact process. Under this condition, IZOD bars with higher flexural stiffness would absorb more energy during bending process and thus cause higher impact strength. However, this could not play an important role since the flexural stiffness of dynamic samples is only slight higher than that of static ones. More importantly, the existence of stretched and oriented rubber particles would affect the propagation of cracks during impact process. Fig. 10 shows the SEM micrographs of fractured surface of blends with 20 wt% rubber content. One can view the formation of the striations left behind on the fracture surface parallel to the crack front as a surface layer buckling process occurring during compressive accommodation of the previously stretched crack front material. Muratoglu et al. had studied the parameters affecting the striation spacing and they concluded that the distance between the striations increases with decreasing crack velocity [39]. Observed from Fig. 10 it is clear that the striation spacing of dynamic specimens in shear layer is larger than that of static specimens in core layer which implies the stretched and oriented rubber particles are more efficient in slowing down the crack propagation velocity compared with the spherical ones and thus causes higher impact strength of dynamic specimens. Fig. 11 shows a schematic representation of the failure mechanism. For static specimens with spherical rubber particles, the crack propagates more easily across the section than it does for dynamic specimens with stretched and oriented rubber particles.

In this paper, what deserved to pay more attention is the orientation direction of the cigar-like rubber particles is perpendicular to the crack propagation direction since the impact strength has dependence on the angle between the orientation direction of stretched rubber particles and the fracture propagation direction, as studied by Wang et al. [40]. Obviously, the stretched rubber particles will cause a strong concentration of stress at the tip. Since the fracture direction also play roles to determine the impact strength, further fracture experiments are needed on specimens with different orientation with respect to the fracture propagation direction. To do this, a rectangle specimen dimension, instead of dumbbell shape is needed, which allows one to get the impact strength both parallel and perpendicular to the shear flow directions. This work is now undertaking in our group.

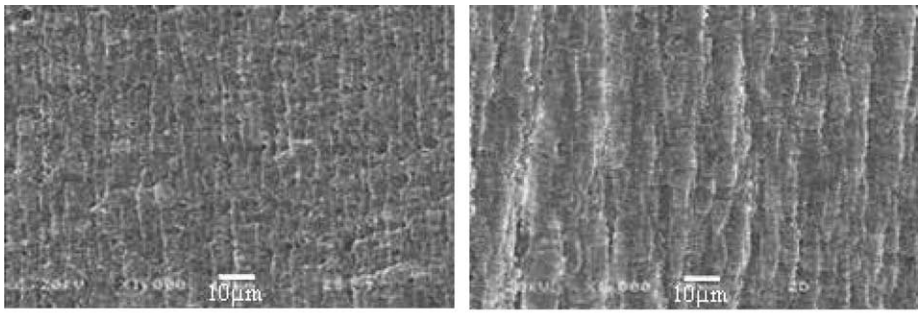

Fig. 10. The SEM photographs of the fracture surface of PA6/EPDM-*g*-MA blends with 20 wt% rubber content. (a) Static specimens in core layer; (b) dynamic specimens in shear layer.

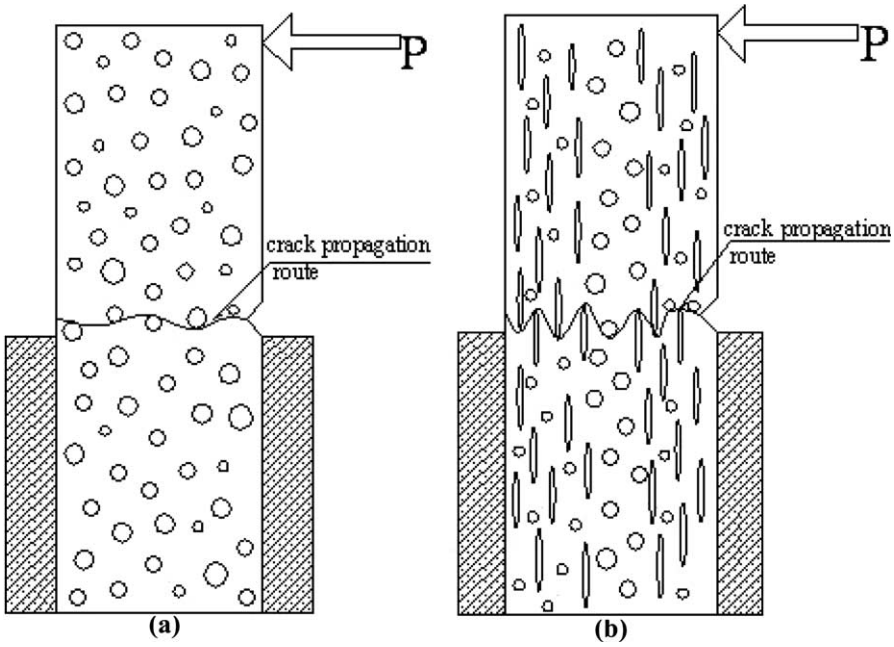

Fig. 11. Schematic representations of the impact fracture mechanism: (a) static specimens; (b) dynamic specimens.

5. Conclusion

The effect of stretched and oriented rubber particles on impact strength of PA6/EPDM-*g*-MA blends is demonstrated in this work. The impact strength obtained by DPIM is higher than that obtained via conventional injection molding, especially, for specimens with higher rubber content. The change of crystal structure between dynamic specimens and static ones does not contribute to the improvement of the impact strength. And the crystalline properties keeps almost constant, disregarding rubber content, injection molding mode, in the shear layer or in the core. So the difference of the impact strength between dynamic and static specimens should be mainly attributed to the difference of phase morphology, considering that the identical impact strength of static and dynamic specimen for pure polyamide 6. The SEM micrographs turn out that cigar-like dispersed phase morphology appears via DPIM when the rubber content exceeds 15 wt% and spherical dispersed phase morphology exists in the composition investigated via traditional injection molding. A master curve can be also constructed by plotting the impact strength versus the inter-particle distance, indicating that Wu's criterion still work for blends with stretched and oriented rubber particles. The increased impact strength could be mainly caused by the existence of the stretched and oriented rubber particles in the dynamic samples, which are more efficient in slowing the velocity of crack propagation and thus cause higher impact resistance when the fracture propagation direction is perpendicular to the rubber oriented direction. The slight higher flexural stiffness in dynamic samples may also contribute a small part of the increase of impact strength when the fracture of IZOD bars is incomplete.

Acknowledgements

We would like to express our sincere thanks to the National Natural Science Foundation of China for Financial Support (20404008, 50533050, 50373030 and 20490220). This work was subsidized by the Special Funds for Major State Basic Research Projects of China (2003CB615600) and by Ministry of Education of China as a key project (104154).

References

[1] Wu S. Polymer 1985;26:1855.
[2] Wu S. J Appl Polym Sci 1988;35:549.
[3] Margolina A, Wu S. Polymer 1988;29:2170.
[4] Borggreve RJM, Gaymans RJ. Polymer 1989;30:63.
[5] Oshinski AJ, Keskkula H, Paul DR. Polymer 1992;33:267.
[6] Majumdar B, Keskkula H, Paul DR. Polymer 1994;35:1399.
[7] Dijkstra K, Ter Laak J, Gaymans RJ. Polymer 1994;35:332.
[8] Borggreve RJM, Gaymans RJ, Schuijer J, Ingen Housz JF. Polymer 1987; 28:1489.
[9] Muratoglu OK, Argon AS, Cohen RE, Weinberg M. Polymer 1995;36: 921.
[10] Muratoglu OK, Argon AS, Cohen RE, Weinberg M. Polymer 1995;36: 4771.
[11] Zheng WG, Li Q, Qi ZN. Chin Sci Bull 1992;37:904.
[12] Zheng WG, Li Q, Qi ZN. J Polym Eng 1993;12:230.
[13] Muratoglu OK, Argon AS, Cohen RE. Polymer 1995;36:2143.
[16] Fisa B, Favis BD, Bourgeois S. Polym Eng Sci 1990;30:1051.
[17] Ghiam F, White JL. Polym Eng Sci 1991;31:76.
[18] Fellahi S, Fisa B, Favis BD. Polymer 1996;37:2615.
[19] Son Y, Ahn KH, Char K. Polym Eng Sci 2000;40:1385.
[20] Danesi S, Porter RS. Polymer 1978;19:448.
[21] Ho WK, Salovey R. Polym Eng Sci 1981;21:839.
[22] Karger-Kocsis J, Tu H-H, Csikai I. Polym Eng Sci 1987;27:247.
[23] Tsebrenko MV, Rezanova NM. Polym Eng Sci 1980;20:1023.
[24] Min K, White JK. Polym Eng Sci 1984;24:1327.
[25] Kim BK, Do IH. J Appl Polym Sci 1996;60:2207.

[26] Kim BK, Kim MS, Kim KJ. J Appl Polym Sci 1993;48:1271.
[27] Hisamatsu T, Nakano S, Adachi T, Ishikawa M, Iwakura K. Polymer 2000;41:4805.
[28] Allen PS, Bevis MJ, UK Patent 2, 170, 140B; 1986.
[29] Guan Q, Shen KZ, Li J, Zhu J. J Appl Polym Sci 1995;55:1797.
[30] Kalay G, Bevis M. J Polym Sci, Part B: Polym Phys 1997;35:241.
[31] Wang Y, Fu Q, Li QJ, Zhang G, Shen KZ, Wang YZ. J Polym Sci, Part B: Polym Phys 2002;40:2094.
[32] Na B, Zhang Q, Fu Q, Zhang G, Shen KZ. Polymer 2002;43:7367.
[33] Inoue M. J Polym Sci, Part A-2 1969;7:1755.
[34] Yalcin B, Valladares D, Cakmak M. Polymer 2003;44:6916.
[35] Wang K, Liang S, Du RN, Zhang Q, Fu Q. Polymer 2004;45:7959.
[36] Wu CJ, Kuo JF, Chen CY. Polym Eng Sci 1993;33:1333.
[37] Irani RR, Callis CF. Particle size: measurement, interpretation and application. New York: Wiley; 1963.
[38] Liu ZH, Zhang XD, Zhu XG, Qi ZN, Wang FS. Polymer 1997;38:5269.
[39] Muratoglu OK, Argon AS, Cohen RE, Weinberg M. Polymer 1995;36:4778.
[40] Wang Y, Zhang Q, Na B, Du RN, Fu Q, Shen KZ. Polymer 2003;44:4264.